Tunable Negative Thermal Expansion in Layered Perovskites from Quasi-Two-Dimensional Vibrations

Liang-Feng Huang, Xue-Zeng Lu, and James M. Rondinelli*
Department of Materials Science and Engineering, Northwestern University, Evanston, Illinois 60208, USA
(Received 6 March 2016; revised manuscript received 15 July 2016; published 7 September 2016)

We identify a quasi-two-dimensional (quasi-2D) phonon mode in the layered-perovskite $Ca_3Ti_2O_7$, which exhibits an acoustic branch with quadratic dispersion. Using first-principles methods, we show this mode exhibits atomic displacements perpendicular to the layered $[CaTiO_3]_2$ blocks comprising the structure and a negative Grüneisen parameter. Owing to these quasi-2D structural and dynamical features, we find that the mode can be utilized to realize unusual membrane effects, including a tunable negative thermal expansion (NTE) and a rare pressure-independent thermal softening of the bulk modulus. Detailed microscopic analysis shows that the NTE relies on strong intralayer Ti—O covalent bonding and weaker interlayer interactions, which is in contrast to conventional NTE mechanisms for perovskites, such as rigid-unit modes, structural transitions, and electronic or magnetic ordering. The general application of the quasi-2D lattice dynamics opens exciting avenues for the control of lattice dynamical and thermodynamic responses of other complex layered compounds through rational chemical substitution, as we show in $A_3Zr_2O_7$ (A = Ca, Sr), and by heterostructuring.

DOI: 10.1103/PhysRevLett.117.115901

The thermal expansion of materials has been intensively studied for decades owing to its importance in numerous fields [1]. In miniaturized electronic and optical devices, the accumulated thermal stress (strain) from fabrication and during operation may cause component spalling, large resistance variability, and shifts in photoluminescence [2]. Ferroelectric logic and memory devices based on perovskite oxides have been fabricated [3], and thermal expansion of such thin films may be a critical factor determining their future viability in low-power information processing and storage technologies [4]. The perovskite-structured $A_3B_2O_7$ (A = Ca, Sr; B = Ti, Mn, …) Ruddlesden-Popper (RP) oxides with a layered habit have recently drawn interest owing to their intriguing hybrid improper ferroelectricity, magnetoelectric and magnetoelastic responses [5], and their unusual thermal expansion [6,7], which requires a detailed understanding before the material family can be integrated into future devices.

Some amount of negative thermal expansion (NTE) may be beneficial for scaffolding different materials into multicomponent architectures because NTE tends to cancel the usual deleterious positive expansion and helps reduce thermal strain; the latter is well exemplified by the famous Invar alloys [8]. In the RP oxides exhibiting relatively high point symmetries (e.g., the high-temperature *nonpolar* phase of $Ca_3Mn_2O_7$; see Ref. [6]), the rigid (quasirigid) unit modes [9] are active, resulting in observable NTE. Although structural, magnetic, and orbital-order transitions can also induce NTE in perovskite-derived compounds, e.g., $BaTiO_3$ [10], $PbTiO_3$ [11], $BiNiO_3$ [12], and $Ca_{n+1}Ru_nO_{3n+1}$ [13,14], all of these NTE-causing factors are absent in the layered RP $Ca_3Ti_2O_7$: (1) The rigid-unit modes are locked [6,9] due to the low orthorhombic symmetry of the crystal, i.e., $Cmc2_1$ [15], (2) there is no temperature-dependent structural transition up to 1150 K [6], at which point the crystal decomposes, and (3) it is nonmagnetic and lacks an orbital-order transition owing to the empty $3d^0$ configuration of the Ti^{4+} cation.

In this Letter, we propose and computationally demonstrate a quasi-two-dimensional (quasi-2D) mechanism for NTE in layered RP oxides, utilizing our recently implemented self-consistent quasiharmonic approximation (SC QHA) method to treat the lattice anharmonicity within a density functional theory (DFT) framework. In the prototypical layered ferroelectric $Ca_3Ti_2O_7$ (CTO), we discover a quasi-2D vibrational mode in the *polar* phase by discerning an acoustic branch with a quadratic dispersion, which appears in the intensely studied 2D materials, e.g., graphene and MoS_2 [16,17]. The quasi-2D vibration resembles the bending vibration on a 2D membrane; we show that this feature results in various extraordinary *membrane effects* in CTO, including negative mode Grüneisen parameters (γ^-) and the enlargement of γ^- by hydrostatic pressure. The membrane effect originally predicted by Lifshitz [18] over 60 years ago endows CTO with tunable NTE, which can be considerably amplified by modest pressures (< 30 GPa here) and also results in an unusual pressure-independent thermal softening of the bulk modulus. We show the mechanism is general and active in other RP oxides, $A_3Zr_2O_7$ (A = Ca, Sr), with the NTE being tuned by the strength of the metal-oxygen bonds.

We calculate the temperature- and pressure-dependent isothermal volume $V_T(P,T)$ of CTO using our SC QHA method [19] and DFT calculations with the Vienna *ab initio*

simulation package (VASP) [20]. In the SC QHA method, an analytical nonlinear frequency–volume relationship is used to solve for $V_T(P,T)$ in an efficient iterative manner; it requires fewer phonon calculations than the conventional QHA method. Furthermore, the SC QHA method avoids the problem of spurious imaginary modes appearing in some expanded volumes of $Ca_3Ti_2O_7$, which prohibits the application of the conventional QHA method [19]. Additional details of the DFT calculations are given in Ref. [21] and structural information is provided in Ref. [25]. To facilitate the microscopic analysis of the anharmonic mechanisms, we express the thermal-expansion coefficient (α) as

$$\alpha = \frac{1}{V}\frac{dV}{dT} = \frac{1}{N_q V_T B_T}\sum_{q,\sigma} C_V^{q,\sigma}\gamma_{q,\sigma}, \quad (1)$$

where q and σ enumerate the phonon wave vector and branch, respectively, N_q is the number of q-grid points ($8\times8\times1$ used here), B_T is the isothermal bulk modulus, C_V is the isovolume heat capacity, and $\gamma = -(V/\nu)(d\nu/dV)$ is the mode Grüneisen parameter for the frequency ν [19]. B_T consists of both electronic (B_e) and phononic (B_ν) contributions, i.e., $B_T = V[d^2(E_e+F_\nu)/dV^2] = B_e + B_\nu$, where E_e and F_ν are the electronic energy and phononic free energy, respectively.

$Ca_3Ti_2O_7$ has a layered orthorhombic structure (Fig. 1, right panel), whereby the perovskite bilayers [$(CaTiO_3)_2$] are separated by the rock salt [CaO] layers along the c axis. The calculated phonon dispersions, atom-, and direction-resolved phonon density of states (g_ν) are shown in Fig. 1. First, we note that the Ti cations are strongly covalently bonded with the O anions, whereas Ca, which provides charge balance and stability to the structure, weakly hybridizes with the TiO_6 octahedra. Thus, g_ν(Ca) mainly occupies the low-frequency region (<13 THz), while g_ν(Ti) has a broader distribution up to 18 THz despite Ti being heavier than Ca. Furthermore, the g_ν(Ti) and $g_\nu(O)$ spectra simultaneously present peaks at various frequencies, indicating a strong vibrational Ti—O coupling through the covalent Ti—O—Ti bond network.

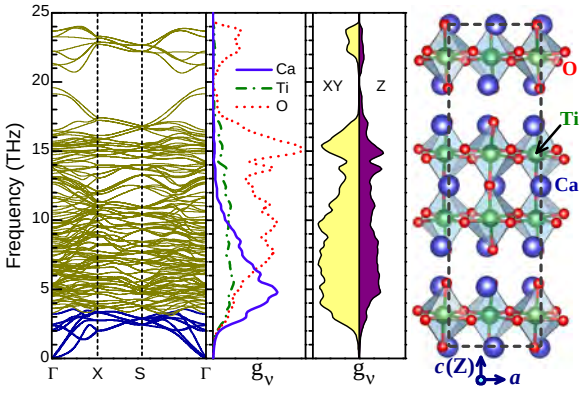

FIG. 1. Phonon dispersions, atom- and direction-resolved phonon density of states (g_ν), and $Ca_3Ti_2O_7$ unit cell where the c axis coincides with the Z direction, and the a and b axes reside in the XY plane. In the left panel, the lowest eight branches containing the quasi-2D vibrations are emphasized by thicker dark blue lines.

Next, in the direction-resolved g_ν, we separate the contributions of the vibrations along the c axis (hereafter, Z vibrations) from those in the ab plane (XY vibrations). The 3D character of the lattice dynamics for $Ca_3Ti_2O_7$ are observed in the wide-range ($XY-Z$)-vibrational coupling; i.e., $g_\nu(XY)$ and $g_\nu(Z)$ have various common peaks owing to the the finite layer thickness and interlayer interactions, as well as to the layer rumpling caused by the octahedral rotation and tilting that yield the hybrid improper ferroelectricity [5]. Apart from this apparent 3D character, we discern a hidden 2D character in the phonon dispersions (Fig. 1, left panel): The lowest acoustic branch along the $\Gamma-X$ path (i.e., $[\xi,0,0]$ path, $\xi\in[0,\frac{1}{2}]$) exhibits a quadratic dispersion. Similar quadratic acoustic modes are ubiquitous in 2D materials [16,17], which have an important phonon mode with largely Z character that is referred to as the ZA mode. The ZA mode in such 2D materials resembles a bending vibration on a continuum membrane or guitar string, and tensile strain can stiffen this bending vibration [9,16], resulting in a negative Grüneisen parameter (γ^-) of the ZA mode that is responsible for the NTE reported in 2D materials. The existence of γ^- and NTE are ascribed to membrane effects [16] (or guitar-string effects [9]). In the following, we reveal various extraordinary membrane effects in CTO, including γ^- and NTE, that originate from the quasi-2D vibrations therein.

We now examine the mode Grüneisen dispersions for CTO [Fig. 2(a)], with a special focus on the ν and γ dispersions of the lowest eight phonon branches in Figs. 2(b) and 2(c), respectively, where the variation of the line width indicates the relative Z-vibration contribution to the mode. The atomic displacements in the quadratic ZA mode and a shearing optical mode (SO mode described later) along the $\Gamma-X$ path are illustrated in Figs. 2(d) and 2(e), respectively. In contrast to the ZA mode in 2D materials, which have large *negative* γ (i.e., γ^-) at the Γ point [16,17], the quasi-2D ZA mode in CTO exhibits a large *positive* γ (γ^+) at the Γ point, and a $\gamma^+\rightarrow\gamma^-$ transition only occurs when approaching the X point [Figs. 2(a) and 2(c)]. Such positive sign and large value of γ^+ at the Γ point both originate from the softness (low ν) of the quadratic ZA mode: Indeed, first there is a stretching of the weak interlayer bonds induced by the ZA mode, and it has been found that bond stretching has a positive contribution to γ [9,17], which becomes important when the ZA mode is soft enough and results in a positive γ despite a quasi-2D quadratic phonon mode dispersion being retained. Second, a soft mode always has a high sensitivity to an external perturbation, e.g., volume compression

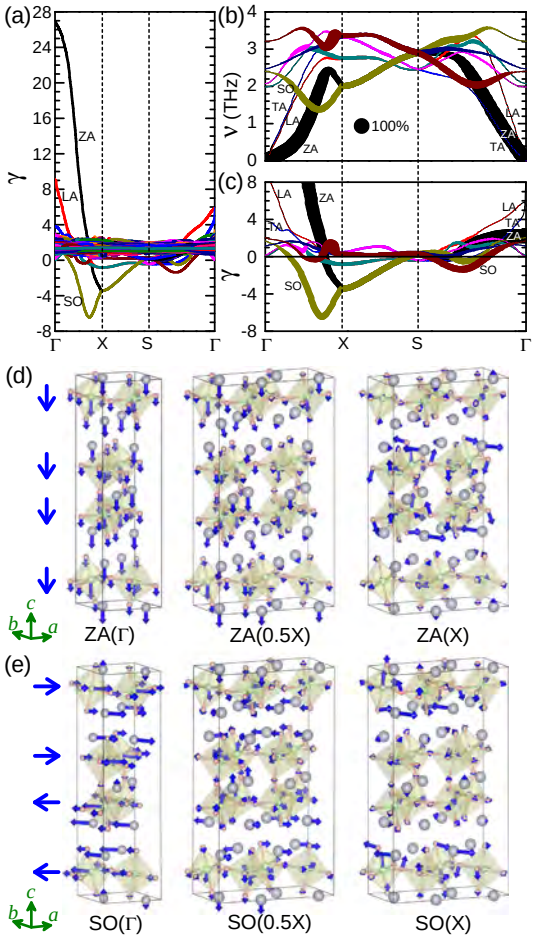

FIG. 2. (a) Full γ dispersions, [(b),(c)] ν and γ dispersions for the lowest eight phonon branches, and [(d),(e)] atomic displacement patterns for the ZA and SO modes at the Γ, $\frac{1}{2}X$, and X points. In panels (b),(c), the line width indicates the contribution of the Z vibration. In panels (d),(e), the overall octahedral-layer displacement directions for the ZA and SO modes at Γ point are indicated by the arrows on the left.

explored below, resulting in the large value of $\gamma^{+}(ZA)$. Along the $\Gamma-S$ path (S: $[\frac{1}{2},\frac{1}{2},0]$), we find that the ZA mode has a greater linear $\nu(q)$ dispersion [Fig. 2(b)] and much smaller γ^{+} (or γ^{-}) [see Fig. 2(c)] than those along the $\Gamma-X$ path, indicating an anisotropic quasi-2D character of the ZA mode in CTO, which should closely correlate with the crystal-structure anisotropy.

Along the $\Gamma-X$ path, $\nu(ZA)$ increases and approaches other acoustic and optical modes at higher frequencies [Fig. 2(b)], which allows for hybridization of the ZA mode with those others of different character. This vibrational mode mixing transfers the quasi-2D Z displacements from the ZA mode to the other modes, especially to the SO mode [Fig. 2(b)]. At the Γ point, the SO mode only consists of XY displacements and each perovskite bilayer in the RP structure makes a shearing distortion [Fig. 2(e)]; however, away from Γ, the quasi-2D Z vibration increases, which results in the $\gamma^{+}\rightarrow\gamma^{-}$ transition [Fig. 2(c)]. Other low-frequency optical modes behave similarly, exhibiting γ^{-}, for the same reasons, while those modes with frequencies higher than the lowest eight phonons only have positive Grüneisen parameters γ^{+} because they are energetically too far away to hybridize with the quasi-2D ZA mode.

The quasi-2D physical picture established above guides us to use hydrostatic pressure to amplify the membrane effect in the phonon anharmonicities and thermodynamic properties of CTO, which (i) furthers our understanding of the quasi-2D character of the mode and (ii) allows us to realize tunable NTE in CTO using a facile approach for future experimental validation.

We now examine the thermal-expansion behavior of CTO subjected to hydrostatic pressures up to 30 GPa [33]. To decipher the average pressure effect on the phonon modes throughout the Brillouin zone, we compute the $\gamma^{\pm}$-weighted phonon density of states ($g_{\gamma^{\pm}}$) defined as

$$g_{\gamma^{\pm}}(\nu)=\frac{1}{N_q}\sum_{q,\sigma}\gamma^{\pm}_{q,\sigma}\delta(\nu-\nu_{q,\sigma}).$$

The pressure-dependent $g_{\gamma^{\pm}}$, their summations over frequency, and peak positions in the $g_{\gamma^{-}}$ spectra are shown in Figs. 3(a)–3(c). At 0 GPa, g^{+}_{γ} prevails over $g_{\gamma^{-}}$ at any ν, and the finite and peaked $g^{+}_{\gamma}(\nu)$ at low ν ($\lesssim$1.0 THz) are mainly due to the large $\gamma^{+}(ZA)$ around the Γ point [Fig. 2(a)]. A finite $g_{\gamma^{-}}$ is only observable between 1.0 and 3.5 THz with two well-defined peaks at 1.8 and 2.7 THz [Fig. 3(a), inset], which originate from the large γ^{-}(SO) and $\gamma^{-}(ZA)$ [Fig. 2(c)], respectively.

At 20 GPa, most phonon modes blueshift to higher frequencies as expected owing to their 3D character and positive γ. The key exceptions are those quasi-2D modes with γ^{-}. The SO and ZA peaks in the $g_{\gamma^{-}}$ spectra shift down to 0.6 and 2.6 THz, respectively, and $g_{\gamma^{-}}$ exceeds g^{+}_{γ} in the low-frequency region ($\lesssim$4.0 THz). Pressure also considerably increases the widths and heights of the $g_{\gamma^{-}}$ peaks, resulting in the rapid decrease of the $g_{\gamma^{-}}$ summation [Fig. 3(b)]. The SO peak shifts to lower frequency faster, but its intensity increases slower than the ZA peak, with increasing pressure [Figs. 3(a) and 3(c)].

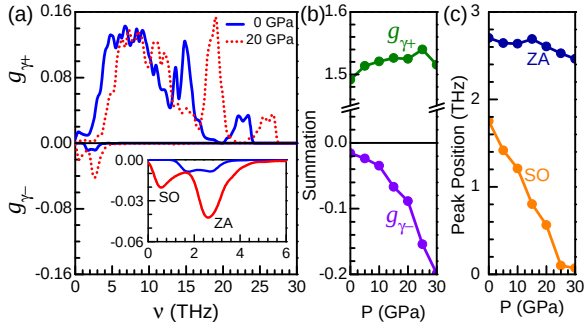

FIG. 3. The variations of (a) $g_{\gamma^{\pm}}$ spectra, (b) $g_{\gamma^{\pm}}$ summations, and (c) $g_{\gamma^{-}}$ peak positions with pressure. In panel (a), the inset enlarges the $g_{\gamma^{-}}$ spectra at low frequencies.

We can understand the ν decrease [Fig. 3(c)] and g_{γ^-} enhancement [Fig. 3(b)] of the quasi-2D modes within the membrane effect as follows: The shrinkage of the perovskite layers (by 0.096 Å^2/GPa per unit cell) makes the quasi-2D modes softer (i.e., lower ν) and more sensitive to the volume compression (i.e., larger γ^-). On the other hand, pressure shortens the interlayer spacing (by 4.6×10^{-3} Å/GPa) and increases the interlayer repulsion, which hardens those ultrasoft ZA modes having γ^+ near the Γ point. Such mode hardening reduces the anharmonicity of those ZA modes, resulting in the decrease of γ^+ and the elimination of the low-frequency g_{γ^+} peak ($\lesssim$1.0 THz) at 20 GPa [Fig. 3(a)].

These unusual pressure-dependent quasi-2D phonon anharmonicities have profound effects on the thermal expansion and thermomechanics of CTO. The calculated $\alpha(T)$ clearly presents a monotonic decrease with increasing pressure [Fig. 4(a)], decreasing by about 50% from 0 to 30 GPa at $\gtrsim$500 K. According to Eq. (1), the bulk modulus (B_T), volume (V_T), heat capacity (C_V), and phonon anharmonicity (γ) collectively determine the thermal-expansion coefficient. Above 500 K, the pressure-induced stiffening in B_T is ~100%, while V_T and C_V only decrease by ~14% and ~2%, respectively [25]. Thus, at high temperatures, pressure suppresses the thermal expansion of CTO primarily through the mechanical stiffening—increase in B_T—which is consistent with the intuitive concept that stiffer lattices are less perturbed by heat.

The mechanical stiffening is also the main cause for the thermal-expansion suppression at temperatures down to 100 K, below which the quasi-2D anharmonicity will dominate. There is only positive thermal expansion ($\alpha > 0$) in CTO at ambient condition (~0 GPa); however, NTE ($\alpha < 0$) appears at pressures >10 GPa and becomes more prominent at higher pressures [Fig. 4(b)]. This response occurs because of the enhanced g_{γ^-} with increasing pressure [Figs. 3(a) and 3(b)], which is a manifestation of the membrane effect described above. Thus, thermal excitation of the γ^- modes becomes more important for α, and the critical temperature T_c defined as $\alpha(T_c) = 0$ also increases with increasing pressure [Fig. 4(b)], reaching 105 K at the phase-stability critical pressure (i.e., 35 GPa). At the NTE critical pressure of 10 GPa, we also find that α becomes negative first at 23 K but remains positive at both lower and higher temperatures. This is because at low pressures, the low-frequency acoustic modes with large γ^+ are excited first, i.e., prior to the excitation of the ZA and SO modes with large γ^- [Figs. 2(a)–2(c)].

The quasi-2D γ^- modes in CTO also have an unusual effect on its pressure-dependent thermomechanics. The thermal softening of the bulk modulus of solids is usually expected to monotonically decrease with increasing pressure, owing to the decreased thermal expansion [19]. However, in CTO, the thermal softening of B_T given as $\Delta B_T = B_T(T) - B_T(0)$ becomes rather pressure independent between 10 and 30 GPa over the entire temperature range considered [Fig. 4(c)] and even becomes very large at the phase-stability critical pressure of 35 GPa. B_T consists of electronic (B_e) and phononic (B_ν) contributions, where B_e behaves as usual with a reduced thermal softening by pressure; however, the thermal softening of B_ν starts to enlarge significantly above 10 GPa [25]. B_ν cancels the reverse variation in the B_e softening and makes ΔB_T quite pressure independent at 10–30 GPa and negatively large at 35 GPa. Although the γ^- modes are only important for α at temperatures $\lesssim T_c$, they nonetheless have a critical effect on ΔB_T at higher temperatures.

The quasi-2D γ^- modes, pressure-induced NTE, and unusual thermal softening of B_T proposed here may be validated by various experimental methods. The pressures of $\lesssim$ 30 GPa are relatively low compared to current experimental upper limits realized in a diamond anvil cell (400 GPa [34]), indicating a facile experimental validation. The quadratic dispersion of the ZA mode can be measured by inelastic x-ray or neutron scattering [16], and the negative γ's of the ZA and SO modes can be derived from their pressure-dependent ν dispersions. The pressure-dependent thermal-expansion coefficient

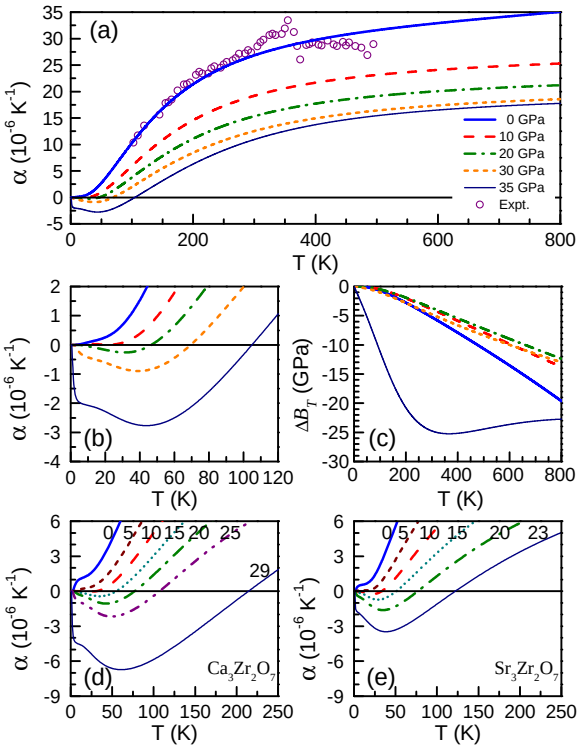

FIG. 4. Pressure-dependent (a) and (b) thermal-expansion coefficient (α) of $Ca_3Ti_2O_7$ (see Refs. [6,19] for experimental data at 0 GPa), (c) bulk-modulus thermal softening (ΔB_T) of $Ca_3Ti_2O_7$, and thermal-expansion coefficients of (d) $Ca_3Zr_2O_7$ and (e) $Sr_3Zr_2O_7$. The results at the phase-stability critical pressures (i.e., 35, 29, and 23 GPa) are also shown. See Ref. [25] for more details about various thermodynamic properties.

($\alpha = (1/V)(dV/dT)$) and isothermal bulk modulus ($B_T = -V(dP/dV)$) can be directly measured using *in situ* x-ray diffraction [34].

According to our analysis on $Ca_3Ti_2O_7$ above, the interlayer interaction, layer thickness, vibrational hybridization, and bond strength are important factors determining the degree of the quasi-2D character in RP perovskites, which indicates an ample space to control their NTE, e.g., utilizing chemical substitution, superlattice engineering, and epitaxial strain in thin films. Guided by this understanding, we calculated the properties of $Ca_3Zr_2O_7$ and $Sr_3Zr_2O_7$ which exhibit the same polar $Cmc2_1$ phase [5] and found larger quasi-2D NTEs appearing at lower pressures [Figs. 4(d) and 4(e)] because the metal-oxygen bond weakening from Zr and Sr substitutions promotes quasi-2D NTE [17,25]. Additional lattice dynamical and thermodynamic properties are provided in Ref. [25].

Last, we compared the quasi-2D properties of different RP perovskites, among which structural and chemical variations can change the active microscopic NTE mechanism. Recent studies on layered $Ca_{3-x}Sr_xMn_2O_7$ ($x = 0$–3) [6,7] show that the polar phase exhibits no NTE down to 90 K, whereas the NTE of the nonpolar state (stabilized by finite temperature or Sr addition) is ascribed to activated rigid-unit modes. The existence of the quasi-2D NTE in different centric and noncentrosymmetric phases of $Ca_{3-x}Sr_xMn_2O_7$ under various external conditions remains unclear. We hope that our finding of quasi-2D physics in the phonon properties and tunable NTE motivate the synthesis and detailed lattice dynamical study of layered oxides exhibiting coupled modes that produce hybrid improper ferroelectricity.

L.-F. H. and J. M. R. wish to thank Dr. M. Senn (Oxford), Professor S.-W. Cheong (Rutgers), and Dr. M.-Q. Gu (Northwestern) for helpful discussions. L.-F. H. was supported by ONR (Grant No. N00014-14-1-0675). X.-Z. L. and J. M. R. were supported by NSF (Grant No. DMR-1420620) and the Alfred P. Sloan Foundation (Award No. FG-2016-6469), respectively. Calculations were performed using the QUEST HPC Facility at Northwestern and the HPCMP facilities at the Navy DSRC.

*jrondinelli@northwestern.edu

[1] C. Romao, K. Miller, C. Whitman, M. White, and B. Marinkovic, in *Comprehensive Inorganic Chemistry II*, 2nd ed., edited by K. R. Poeppelmeier and J. Reedijk (Elsevier, Amsterdam, 2013), pp. 127–151.

[2] G. Plechinger, F.-X. Schrettenbrunner, J. Eroms, D. Weiss, C. Schüller, and T. Korn, Phys. Status Solidi (RRL) **6**, 126 (2012); K. Sano, T. Takahashi, and K. Uchida, Jpn J. Appl. Phys. **55**, 036501 (2016).

[3] M. P. Warusawithana, C. Cen, C. R. Sleasman, J. C. Woicik, Y. Li, L. F. Kourkoutis, J. A. Klug, H. Li, P. Ryan, L.-P. Wang, M. Bedzyk, D. A. Muller, L.-Q. Chen, J. Levy, and D. G. Schlom, Science **324**, 367 (2009); V. Garcia and M. Bibes, Nat. Commun. **5**, 4289 (2014).

[4] J. M. Rondinelli, K. R. Poeppelmeier, and A. Zunger, APL Mater. **3**, 080702 (2015).

[5] N. A. Benedek and C. J. Fennie, Phys. Rev. Lett. **106**, 107204 (2011); N. A. Benedek, A. T. Mulder, and C. J. Fennie, J. Solid State Chem. **195**, 11 (2012); A. T. Mulder, N. A. Benedek, J. M. Rondinelli, and C. J. Fennie, Adv. Funct. Mater. **23**, 4810 (2013); N. A. Benedek, J. M. Rondinelli, H. Djani, P. Ghosez, and P. Lightfoot, Dalton Trans. **44**, 10543 (2015); Y. S. Oh, X. Luo, F.-T. Huang, Y. Wang, and S.-W. Cheong, Nat. Mater. **14**, 407 (2015).

[6] M. S. Senn, A. Bombardi, C. A. Murray, C. Vecchini, A. Scherillo, X. Luo, and S. W. Cheong, Phys. Rev. Lett. **114**, 035701 (2015).

[7] M. S. Senn, C. Murray, X. Luo, L. Wang, F.-T. Huang, S.-W. Cheong, A. Bombardi, C. Ablitt, A. A. Mostofi, and N. C. Bristowe, J. Am. Chem. Soc. **138**, 5479 (2016).

[8] T. Yokoyama and K. Eguchi, Phys. Rev. Lett. **110**, 075901 (2013).

[9] G. D. Barrera, J. A. O. Bruno, T. H. K. Barron, and N. L. Allan, J. Phys. Condens. Matter **17**, R217 (2005); B. Fultz, Prog. Mater. Sci. **55**, 247 (2010); C. Lind, Materials **5**, 1125 (2012).

[10] S. Sawada and G. Shirane, J. Phys. Soc. Jpn. **4**, 52 (1949).

[11] G. Shirane and S. Hoshino, J. Phys. Soc. Jpn. **6**, 265 (1951); J. Kobayashi, Y. Uesu, and Y. Sakemi, Phys. Rev. B **28**, 3866 (1983); J. Chen, L. Fan, Y. Ren, Z. Pan, J. Deng, R. Yu, and X. Xing, Phys. Rev. Lett. **110**, 115901 (2013); H. Fang, Y. Wang, S. Shang, and Z.-K. Liu, Phys. Rev. B **91**, 024104 (2015).

[12] M. Azuma, W.-T. Chen, H. Seki, M. Czapski, K. Oka, M. Mizumaki, T. Watanuki, N. Ishimatsu, N. Kawamura, S. Ishiwata *et al.*, Nat. Commun. **2**, 347 (2011).

[13] Y. Yoshida, S.-I. Ikeda, H. Matsuhata, N. Shirakawa, C. H. Lee, and S. Katano, Phys. Rev. B **72**, 054412 (2005).

[14] T. F. Qi, O. B. Korneta, S. Parkin, L. E. De Long, P. Schlottmann, and G. Cao, Phys. Rev. Lett. **105**, 177203 (2010); T. F. Qi, O. B. Korneta, S. Parkin, J. Hu, and G. Cao, Phys. Rev. B **85**, 165143 (2012).

[15] M. M. Elcombe, E. H. Kisi, K. D. Hawkins, T. J. White, P. Goodman, and S. Matheson, Acta Crystallogr. Sect. B **47**, 305 (1991); A. B. Harris, Phys. Rev. B **84**, 064116 (2011).

[16] N. Mounet and N. Marzari, Phys. Rev. B **71**, 205214 (2005).

[17] L.-F. Huang and Z. Zeng, J. Phys. Chem. C **119**, 18779 (2015).

[18] I. M. Lifshitz, Zh. Eksp. Teor. Fiz. **22**, 475 (1952).

[19] L. F. Huang, X. Z. Lu, E. Tennessen, and J. M. Rondinelli, Comput. Mater. Sci. **120**, 84 (2016).

[20] J. Hafner, J. Comput. Chem. **29**, 2044 (2008).

[21] We used the PBEsol functional [22] and Ca, Ti, and O pseudopotentials with valence configurations of $3s^23p^64s^2$, $3p^63d^24s^2$, and $2s^22p^4$ within the projector augmented-wave method [23]. The phonon spectra are calculated using the PHONOPY code [24], where the small-displacement method is implemented using amplitudes of 0.03 Å in a $2 \times 2 \times 1$ supercell. The plane wave is expanded up to 800 eV, and the reciprocal grids for the unit cell and supercell are $4 \times 4 \times 2$ and $2 \times 2 \times 2$, respectively. The energy convergence threshold is 10^{-8} eV.

[22] J. P. Perdew, A. Ruzsinszky, G. I. Csonka, O. A. Vydrov, G. E. Scuseria, L. A. Constantin, X. Zhou, and K. Burke, Phys. Rev. Lett. **100**, 136406 (2008).
[23] P. E. Blöchl, Phys. Rev. B **50**, 17953 (1994); G. Kresse and D. Joubert, Phys. Rev. B **59**, 1758 (1999).
[24] A. Togo and I. Tanaka, Scr. Mater. **108**, 1 (2015).
[25] See the Supplemental Material at http://link.aps.org/supplemental/10.1103/PhysRevLett.117.115901 for more details about structures, phonons, and thermodynamic properties, which includes Refs. [25–31].
[26] S.-L. Shang, Y. Wang, D. Kim, and Z.-K. Liu, Comput. Mater. Sci. **47**, 1040 (2010).
[27] A. Glensk, B. Grabowski, T. Hickel, and J. Neugebauer, Phys. Rev. X **4**, 011018 (2014).
[28] T. Noguchi, T. Okubo, and O. Yonemochi, J. Am. Ceram. Soc. **52**, 178 (1969).
[29] F. W. Poulsen and N. van der Puil, Solid State Ionics **53–56**, 777 (1992).
[30] A. Banerjee, S. Dash, R. Prasad, and V. Venugopal, J. Alloys Compd. **267**, 19 (1998).
[31] S. Roitti, J. Mater. Sci. Lett. **1**, 217 (1982).
[32] V. Longo and D. Minichelli, Ceramurgia **4**, 25 (1974).
[33] The SO mode becomes imaginary under a pressure of $\gtrsim$35 GPa, indicating a dynamical instability of $Ca_3Ti_2O_7$ against an intralayer shearing reconstruction [Fig. 2(e)].
[34] R. Boehler, Rev. Geophys. **38**, 221 (2000); P. Dalladay-Simpson, R. T. Howie, and E. Gregoryanz, Nature (London) **529**, 63 (2016).